BALKAN JOURNAL OF ELECTRICAL & COMPUTER ENGINEERING, Vol. 12, No. 3, September 2024

Multipath Characteristics of Orbital Angular Momentum Vortex Electromagnetic Radio Waves Over an Infinite Ground Plane

Ugur Yesilyurt

***Abstract*—In this paper, the effect of an infinitely sized ground plane on the orbital angular momentum (OAM) vortex electromagnetic (EM) radio waves is investigated. Although the effect of an infinite ground on OAM wave propagation and communication has already been numerically examined in the literature using the method of moments (MoM), this study analyzes this situation analytically and obtains the final form expressions derived theoretically. The multipath characteristics of OAM waves in a superconducting ground plane are theoretically presented considering both horizontal and vertical polarization conditions. In addition to direct radiation to an observation point in the far-field from the array antenna, many reflected radiations from the ground plane are also transmitted. The most fundamental reflected radiation is analyzed over a uniform circular array (UCA), adopting electromagnetic image theory. Furthermore, the transmitted field expressions obtained by considering both the circular array parallel to the ground plane and the circular array upright to the ground plane are formulated in a general analytical form for an OAM wave on a superconducting ground plane. In addition, numerical simulations are applied to exemplify the properties of OAM waves in the superconducting ground plane, unlike the isolated medium.**

***Index Terms*—Antenna arrays, infinite ground plane, orbital angular momentum (OAM), multipath propagation.**

I. Introduction

BESIDES linear momentum, an electromagnetic (EM) wave can carry two types of angular momentum related to rotational dynamics: spin angular momentum and orbital angular momentum. Unlike spin angular momentum (SAM), which describes the polarization state of electromagnetic radiation, orbital angular momentum (OAM) is concerned with spatial phase distribution. OAM, which has a special physical property in addition to conventional linear momentum and SAM, can offer new degrees of freedom [1], [2], [3], [4]. Thus, the vortex electromagnetic waves carrying OAM have been a rapidly growing area of research that has attracted great interest in many fields over the past few years. Different from frequency, time, phase, amplitude, and polarization, OAM, which is a new degree of freedom, has distinctive advantages such as secure transmission and information transmission speed and capacity [5], [6], [7], [8], [9], [10], [11].

An OAM vortex EM wave is usually an EM wave with a ”doughnut”-like intensity shape where the electric field intensity is zero at the center. Compared to plane waves, EM waves carrying OAM possess a spiral wave phase front structure. For this reason, EM waves carrying OAM are frequently referred to as spiral, vortex, helical, or twisting waves. Phase fronts with different OAM modes generate different spiral electromagnetic waves. The modes of OAM are mutually orthogonal to each other, and this orthogonality greatly increases the efficiency of spectrum utilization and degrees of freedom [12], [13], [14], [15], [16].

After the investigation in 1992 that helical phase-fronted light beams can carry the OAM, the vortex EM waves have been widely used in optics [12]. B. Thid´e et al. demonstrated that OAM is not limited to electromagnetic waves at light frequencies, by introducing the operation of OAM beams to the radio frequency (RF) field for the first time in 2007 [17]. Thus the potential of using OAM for communication has found application in the range of radio frequencies lower than light. Many methods have been improved in the literature to produce OAM radio waves, including antenna arrays, spiral reflectors, spiral phase plates, and metasurface [18], [19], [20], [21], [22]. Furthermore, due to its high controllability and good beamforming ability, a uniform circular array (UCA) is extensively utilized in OAM beam production. In order to produce an OAM beam in a UCA, the same amplitude and appropriate phase-shifted feed network must be applied to each element. By using incrementally gradual phase generators between adjacent antennas at the UCA, beams with various OAM modes can be generated [23], [24], [25], [26]. In addition, OAM beams are formed using the concentric circular array (CCA) structure, which consists of more than one circular array with different radii and the same center [27], [28]. Unlike UCAs which need external phase shift networks for neighboring elements, it is possible to obtain OAM with helical circular subarray (HCSA) forms with helical phase alignments [29].

Usually, only the direct propagation is analyzed analytically, considering the propagation of the OAM wave in an isolated environment. In real life, unlike an isolated environment, vortex electromagnetic waves not only come from antenna elements directly to the observation point but also reflected waves from the ground plane. Thus, the effect of multipath propagation of vortex EM waves carrying OAM is an important issue to be investigated, and the effect of an infinite ground on OAM wave propagation and communication was studied using the method of moments (MoM) in [30]. In the literature, an analytical investigation of multipath propagation of linear arrays has been made [31], [32]. In this study, the

Ugur Yesilyurt is with the Department of Electrical and Electronic Engineering, Engineering and Architecture Faculty, Erzurum Technical University, Erzurum, 25050, Turkey e-mail: ugur.yesilyurt@erzurum.edu.tr

Manuscript received May 3, 2024; accepted SEp 16, 2024.
DOI: 10.17694/bajece.1477981

 ISSN: 2147-284X https://dergipark.org.tr/bajece

analytical investigation is made for the case where UCA is positioned on the ground plane to examine the effect of an infinite ground on OAM wave propagation. Therefore, interesting simulation results have been obtained by analytically examining the multipath propagation of vortex EM waves in the superconducting ground plane based on a theoretical basis. The multipath properties of OAM waves in a superconducting ground plane, both parallel and upright positioning of the UCA to the ground plane are theoretically evaluated. Contrary to an isolated environment as a result of the constructive and destructive effect of multiple propagations at the observation point, it slices the "donut"-like OAM pattern. Similarly, the vortex EM wave helical phase fronts are also segmented symmetrically with respect to the ground plane normal. In conclusion, this study has contributed to the literature through theoretical investigation and three-dimensional simulations considering the multipath effect of the OAM wave and the ground plane design of the UCA.

II. The Multipath Radiation of OAM Wave over the Infinite Ground Plane

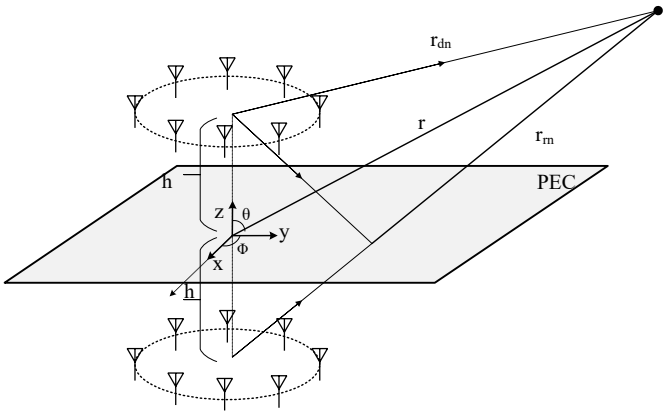

Fig. 1. UCA placed parallel at a given height (h) from an infinitely sized superconducting ground plane

The simple two-way propagation configuration of vortex EM waves carrying OAM is demonstrated in Figure 1. A circular array of N elements is parallel to the ground position along a circular ring of radius a. The UCA has h height from the superconducting ground plane placed in the x-y plane. To achieve the OAM wave, the UCA configuration is basically phased the array with a $2\pi l/N$ phase difference between the elements; where l represents the OAM mode number (topological charge). For the image theory analytical application, hypothetical array elements are constructed symmetrically according to the ground position (depth h below the ground plane) with the approach that the ground plane is infinitely sized superconducting ground. In addition to the direct path to the observation point, there are many reflected paths from the ground plane. The multipath property of the OAM wave, which comprises the direct and the most fundamental reflected path, is examined. The electric field of the OAM wave propagating in the direct path under the far-field approach can be mathematically written as:

$$E_d = \sum_{n=0}^{N-1} I_n \xi_n(\theta_{dn}, \phi_{dn}) \frac{e^{jw_0(t-\frac{r_{dn}}{c})}}{r_{dn}} e^{jl\phi_n}, \quad (1)$$

where, I_n represents n^{th} element excitation amplitude, $\xi_n(\theta_{dn}, \phi_{dn})$ denotes the n^{th} element far-field pattern at the direct path, r_{dn} is the n^{th} array element direct path, and $w_0 = 2\pi f_0$ is the center operating frequency. $\phi_n = 2\pi n/N$ represents the n^{th} element excitation phase ($n = 0, 1, ..., N-1$). In terms of the phase term, the r_{dn} delay term is denoted by

$$r_{dn} \cong r - \langle \hat{\mathbf{a}}_r, \mathbf{r}_n \rangle, \quad (2)$$

where, $\langle ., . \rangle$ denotes the inner product operator, $\hat{\mathbf{a}}_r = sin\theta cos\phi \hat{\mathbf{a}}_x + sin\theta sin\phi \hat{\mathbf{a}}_y + cos\theta \hat{\mathbf{a}}_z$ represents the unit vector in the way of the observation point, and $\mathbf{r}_n = acos\phi_n \hat{\mathbf{a}}_x + asin\phi_n \hat{\mathbf{a}}_y + h\hat{\mathbf{a}}_z$ (where h is the height from the array center to the ground plane and a is the circle radius.) is the position vector for the n^{th} real element of the array. The r_{dn} delay term is denoted by:

$$\begin{aligned} r_{dn} &\cong r - \langle \hat{\mathbf{a}}_r, (acos\phi_n \hat{\mathbf{a}}_x + asin\phi_n \hat{\mathbf{a}}_y + h\hat{\mathbf{a}}_z) \rangle \\ &\cong r - asin\theta cos(\phi - \phi_n) - hcos\theta. \end{aligned} \quad (3)$$

By substituting Equation (3) into Equation (1), the electric field propagating in the direct path of the OAM wave becomes:

$$\begin{aligned} E_d = e^{j\frac{w_0}{c}(tc-r)} \sum_{n=0}^{N-1} I_n \xi_n(\theta_{dn}, \phi_{dn}) \\ \frac{1}{r_{dn}} e^{j\frac{w_0}{c}[asin\theta cos(\phi-\phi_n)+hcos\theta]} e^{jl\phi_n}. \end{aligned} \quad (4)$$

On the other hand, image theory is used to obtain the electric field expression of the most fundamental OAM wave reflected by the ground. The hypothetical array elements are constructed symmetrically according to the ground position (according to image theory), and this OAM wave propagating directly from the hypothetical array antenna to the observation point is equivalent to the most fundamental OAM wave reflected by the superconducting ground plane. In addition, in the horizontal and vertical polarization cases, the hypothetical array antenna polarization is the opposite and the same as the original polarization of the real array antenna, respectively. Therefore, the electric field of the most fundamental OAM wave reflected by the ground is given by:

$$E_r = \underset{v_p}{\overset{h_p}{\mp}} \sum_{n=0}^{N-1} I_n \xi_n(\theta_{rn}, \phi_{rn}) \frac{e^{jw_0(t-\frac{r_{rn}}{c})}}{r_{rn}} e^{jl\phi_n}, \quad (5)$$

where, v_p denotes vertical polarization, and h_p and denotes horizontal polarization. r_{rn} is the direct path to the observation point of UCA's n^{th} hypothetical source, and r_{rn} is also the path of the most fundamental OAM wave reflected from the ground plane. In terms of the phase term of the reflected OAM wave, the r_{rn} delay term is denoted by:

$$r_{rn} \cong r - \langle \hat{\mathbf{a}}_r, \mathbf{r}_n^{'} \rangle, \tag{6}$$

where, $\mathbf{r}_n^{'} = acos\phi_n \hat{\mathbf{a}}_x + asin\phi_n \hat{\mathbf{a}}_y - h\hat{\mathbf{a}}_z$ is the position vector for the n^{th} hypothetical element of UCA. The r_{rn} delay term is given by:

$$\begin{aligned} r_{rn} &\cong r - \langle \hat{\mathbf{a}}_r, (acos\phi_n \hat{\mathbf{a}}_x + asin\phi_n \hat{\mathbf{a}}_y - h\hat{\mathbf{a}}_z) \rangle \\ &\cong r - asin\theta cos(\phi - \phi_n) + hcos\theta. \end{aligned} \tag{7}$$

The electric field directly emitted from the hypothetical UCA is defined as follows by putting the r_{rn} delay term in the Equation (5):

$$\begin{aligned} E_r = \underset{v_p}{\overset{h_p}{\mp}} e^{j\frac{w_0}{c}(tc-r)} \sum_{n=0}^{N-1} I_n \xi_n(\theta_{rn}, \phi_{rn}) \\ \frac{1}{r_{rn}} e^{j\frac{w_0}{c}[asin\theta cos(\phi-\phi_n) - hcos\theta]} e^{jl\phi_n}, \end{aligned} \tag{8}$$

The intervals of the hypothetical and real UCA elements to the observation point can be taken to be approximately ($r_{dn} \approx r_{rn} \approx r$) equal for the amplitude terms under the far-field approach ($r \gg a, h$). Similarly, the element positions of the UCA can be taken the same for the real and hypothetical array elements under the far-field ($\theta_{dn} \approx \theta_{rn} \approx \theta$ and $\phi_{dn} \approx \phi_{rn} \approx \phi$). Considering that all the elements in UCA are identical, the $\xi_n(\theta_{dn}, \phi_{dn})$ and $\xi_n(\theta_{rn}, \phi_{rn})$ expressions can be approximately equated to $\xi(\theta, \phi)$. The total electric field of the OAM waves transmitted to the observation point along both the line-of-sight path and the most fundamental path reflected from the ground plane can be approximately expressed as:

$$\begin{aligned} E_t \approx \frac{e^{j\frac{w_0}{c}(tc-r)}}{r} \sum_{n=0}^{N-1} I_n \xi(\theta, \phi) e^{j\frac{w_0}{c}(asin\theta cos(\phi-\phi_n))} e^{jl\phi_n} \\ \times \left[e^{j\frac{w_0}{c}(hcos\theta)} \underset{v_p}{\overset{h_p}{\mp}} e^{-j\frac{w_0}{c}(hcos\theta)} \right]. \end{aligned} \tag{9}$$

As a result, the expression of the total electric field for vertical and horizontal polarization at the observation point is

$$\begin{aligned} E_t \approx \underbrace{\frac{e^{jk_0(tc-r)}}{r} \xi(\theta, \phi)}_{\text{field of an element}} \underbrace{\sum_{n=0}^{N-1} I_n e^{jk_0(asin\theta cos(\phi-\phi_n))} e^{jl\phi_n}}_{\text{circular array factor}} \\ \times \underbrace{\begin{bmatrix} 2jsin(k_0 hcos\theta)_{h_p} \\ 2cos(k_0 hcos\theta)_{v_p} \end{bmatrix}}_{\text{multipath factor}}. \end{aligned} \tag{10}$$

where $k_0 = w_0/c$ represents the free space wave number.

The total electric field of the UCA located parallel to the superconducting ground plane involves a uniform circular array factor, element field, and multipath factor containing the most fundamental reflected path and the direct path. The multipath factor varies depending on the k_0 free space wave number, the θ elevation angle, and the h height (distance between the ground plane and array), but also changes depending on the polarization (h_p and v_p).

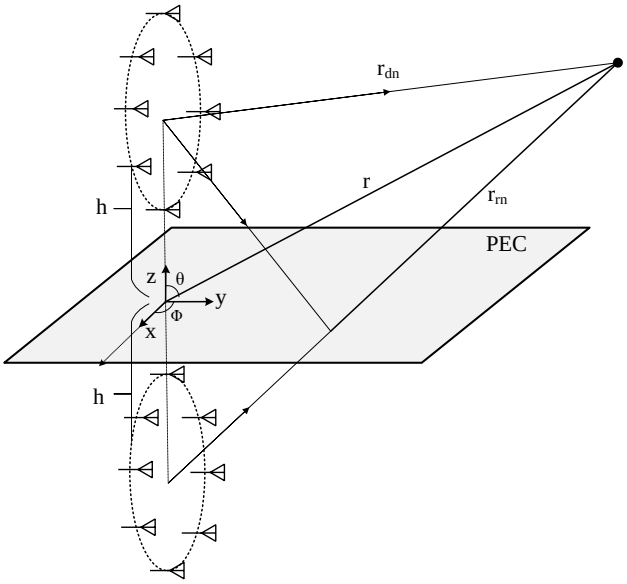

Fig. 2. UCA placed upright at a given height (h) from an infinitely sized superconducting ground plane

As seen in Figure 2, the N-element circular array is located at a h height from the superconducting ground plane and equidistant along a circular ring upright to the ground position. Similarly, the configuration of the UCA basically gives the array with a $2\pi l/N$ phase difference between the neighboring elements to obtain the OAM beam. Also, unlike parallel positioning, upright positioning also occurs symmetrically with respect to the ground position, with hypothetical array elements at different h depths below the ground plane. The OAM electric field propagating along the line of sight under the far-field approach when the UCA is located uprightly to the ground is given as:

$$E_d = \sum_{n=0}^{N-1} I_n \xi_n(\theta_{dn}, \phi_{dn}) \frac{e^{jw_0(t-\frac{r_{dn}}{c})}}{r_{dn}} e^{jl\phi_n}, \tag{11}$$

In terms of the phase term, the $r_{dn} \cong r - \langle \hat{\mathbf{a}}_r, \mathbf{r}_n \rangle$ delay term is given by:

$$\begin{aligned} r_{dn} &\cong r - \langle \hat{\mathbf{a}}_r, (acos\phi_n \hat{\mathbf{a}}_x + (h - asin\phi_n)\hat{\mathbf{a}}_z) \rangle \\ &\cong r - asin\theta cos\phi cos\phi_n + acos\theta sin\phi_n - hcos\theta, \end{aligned} \tag{12}$$

where h is the interval from the array center to the ground plane. The reference plane of the ϕ_n angle is the x-axis. By combining the equation (12) with the equation (11), the electric field expression for the directly propagating OAM wave for the UCA situation located upright to the ground is defined by:

$$E_d = e^{j\frac{w_0}{c}(tc-r)}\sum_{n=0}^{N-1} I_n\xi_n(\theta_{dn},\phi_{dn}) \frac{1}{r_{dn}} e^{j\frac{w_0}{c}[asin\theta cos\phi cos\phi_n - acos\theta sin\phi_n + hcos\theta]} e^{jl\phi_n}, \quad (13)$$

In the situation of UCA located upright to the ground plane, the most fundamental OAM electric field reflected by the ground plane is the same as that of the line-of-sight electric field propagated from the hypothetical arrays. The most fundamental electric field reflected by the ground plane in both the vertical and horizontal polarization states can be expressed as:

$$E_r = \underset{v_p}{\overset{h_p}{\mp}} \sum_{n=0}^{N-1} I_n\xi_n(\theta_{rn},\phi_{rn}) \frac{e^{jw_0(t-\frac{r_{rn}}{c})}}{r_{rn}} e^{jl\phi_n}, \quad (14)$$

In terms of the phase term of the OAM wave reflected from the UCA located upright to the ground plane, the $r_{rn} \cong r - \langle \hat{\mathbf{a}}_r, \mathbf{r}_n^{'} \rangle$ delay term can be expressed as:

$$\begin{aligned} r_{rn} &\cong r - \langle \hat{\mathbf{a}}_r, (acos\phi_n \hat{\mathbf{a}}_x + (-h - asin\phi_n)\hat{\mathbf{a}}_z) \rangle \\ &\cong r - asin\theta cos\phi cos\phi_n + acos\theta sin\phi_n + hcos\theta. \end{aligned} \quad (15)$$

The most fundamental electric field reflected by the ground plane of the UCA located upright to the ground position, together with the r_{rn} delay term, can be expressed as follows:

$$E_r = \underset{v_p}{\overset{h_p}{\mp}} e^{j\frac{w_0}{c}(tc-r)}\sum_{n=0}^{N-1} I_n\xi_n(\theta_{rn},\phi_{rn}) \frac{1}{r_{rn}} e^{j\frac{w_0}{c}[asin\theta cos\phi cos\phi_n - acos\theta sin\phi_n - hcos\theta]} e^{jl\phi_n}, \quad (16)$$

Under the same conditions stated for the parallel placed UCA ($r_{dn} \approx r_{rn} \approx r$ and $\xi_n(\theta_{dn},\phi_{dn}) \approx \xi_n(\theta_{rn},\phi_{rn}) \approx \xi(\theta,\phi)$), the total electric field including the direct and most fundamental reflected radiations of the UCA located upright to the ground position can be expressed as:

$$E_t \approx \frac{e^{j\frac{w_0}{c}(tc-r)}}{r}\sum_{n=0}^{N-1} I_n\xi(\theta,\phi) e^{j\frac{w_0}{c}(asin\theta cos\phi cos\phi_n - acos\theta sin\phi_n)} e^{jl\phi_n} \times \left[e^{j\frac{w_0}{c}(hcos\theta)} \underset{v_p}{\overset{h_p}{\mp}} e^{-j\frac{w_0}{c}(hcos\theta)} \right]. \quad (17)$$

The final electric field at the observing point of the UCA located upright to the ground for vertical and horizontal polarization is expressed by:

$$E_t \approx \underbrace{\frac{e^{jk_0(tc-r)}}{r}\xi(\theta,\phi)}_{\text{field of an element}} \underbrace{\sum_{n=0}^{N-1} I_n e^{jk_0(asin\theta cos\phi cos\phi_n - acos\theta sin\phi_n)} e^{jl\phi_n}}_{\text{circular array factor}} \times \underbrace{\begin{bmatrix} 2jsin(k_0 hcos\theta)_{h_p} \\ 2cos(k_0 hcos\theta)_{v_p} \end{bmatrix}}_{\text{multipath factor}}. \quad (18)$$

The total electric field of the UCA located upright to the superconducting ground plane differs from that of the parallel-located UCA in terms of the circular array factor. The multipath factor with multipath propagation features, which consists of two propagation paths, is the same for both array positions and varies with h height.

Based on the Nyquist sampling theorem, the largest OAM mode l_{max} that the UCA can produce depends on the number of elements in the array. Therefore, the maximum-mode OAM votex beam number that can be obtained from the N-element UCA must satisfy the condition $N \geq 2|l_{max}| + 1$. Therefore, the parameter affecting the maximum number of modes that can be obtained from the OAM is the UCA element number [29].

On the other hand, the number of slices that can be obtained from OAM in the range $\theta \in [0, \frac{\pi}{2}]$ is determined as approximately $\frac{2h}{\lambda} + 1$ and $\frac{2h}{\lambda}$ for vertical and horizontal polarization cases, respectively. Similarly, the parameters that affect the maximum number of slices that can be obtained from OAM are the h height of the array elements from the ground plane and the λ wavelength[31], [32].

The number of UCA elements N and the height h, which is the distance between the ground plane and the array, are of critical importance, as they directly affect the number of users or devices that can be practically multiplexed and served without interference in certain communication systems.

III. Numerical Examples

In this section, numerical examples are given to demonstrate and compare the multipath propagation performances of UCA located parallel and upright to the ground. The results are obtained simply by evaluating the most basic two-way analytical electric fields including the direct and most fundamental reflected constituent in Section 2. To illustrate the multipath characteristic of the OAM wave, let us first consider a parallel-positioned circular array ($a = 0.7\lambda$ radius and $h = 5\lambda$ height) with respect to the infinitely sized superconducting ground plane. The UCA with $f_0 = 5$ GHz center operating frequency is evaluated in the horizontal polarization situation. In addition, the $\phi_n = 2\pi n/N, n = 1, 2, 3, ..., N$ phase is applied to each array element to obtain an OAM wave with the mode-1 ($l = 1$). The effect of frequency on multipath characteristics is present [9]. However, in this study, the height h is given in terms of wavelength λ to study the effect of height. Therefore, the same result is obtained at different frequencies.

As a result of the interference of OAM waves reaching the observing point with the direct and most fundamental reflected path, null values occur that divide the OAM beam into slices. Both the number and position of these nulls that slice the OAM beam in the elevation plane depend on the multipath characteristic (the $2cos(k_0hcos\theta)$ term for the vertical polarization case is the multipath factor and the $2jsin(k_0hcos\theta)$ term for the horizontal polarization case is the multipath factor). UCA's OAM radiation beam varies with the h height between the array and the ground position and the k_0 free space wave number. For the case where the absence of a ground plane, the three-dimensional (r, θ, ϕ) snapshot graph of the OAM beam with mod-1 obtained from the UCA located parallel to the x-y plane at a $h = 5\lambda$ height from the origin is given in the Figure 3(a). In the OAM radiation pattern of the UCA, where there is no ground plane, no nulls are occured in the elevation plane, resulting in a stable OAM wave.

However, slices occur in the OAM radiation beam of the parallel-positioned UCA with respect to the infinitely sized superconducting ground plane. As seen in the three-dimensional (3-D) instantaneous graph in Figure 3(b), more than one ring is formed in the OAM radiation pattern due to the multipath characteristic. The number of these rings varies according to the h height variable between the array and the ground position. The OAM radiation pattern of the parallel-positioned UCA (at a height of $h = 5\lambda$) with respect to the infinitely sized superconducting ground plane is shown in Figure 3(b). Furthermore, with the effect of the multipath characteristic, approximately $\frac{2h}{\lambda} + 1$ and $\frac{2h}{\lambda}$ OAM pattern slices occur in the vertical and horizontal polarization states, respectively, in the $\theta \in [0, \frac{\pi}{2}]$ range. It is seen in the Figure 3(b) that the OAM radiation beam slice number in the $\theta \in [0, \frac{\pi}{2}]$ range of the UCA located parallel at a height of $h = 5\lambda$ for the horizontal polarization case is $\frac{2(5\lambda))}{\lambda} = 10$.

In addition, OAM beams produced by UCA with radius $a = 0.7\lambda$ located at the height of $h = 5\lambda$ from the origin for the isolated medium without ground plane are sampled at $z = 1$km from the origin. The sampled OAM intensity pattern and helical phase wavefronts are illustrated in Figure 4(a) and Figure 4(b), respectively. In both cases, the obtained observation window plane with a width of 1 km in the x-y direction is upright to the beam axis. Figure 4(a) shows that in an isolated medium without a ground plane, a "doughnut" shaped intensity pattern of the $l = 1$ mode OAM wave is obtained. On the other hand, Figure 4(b) shows the spiral phase wavefront for the $l = 1$ mode OAM beam, where the phase change from 0 to 2π corresponds to a change in color from blue to red

By sampling the radiation pattern of the parallel-positioned UCA (radius $a = 0.7\lambda$ and at a height of $h = 5\lambda$) with respect to the infinitely sized superconducting ground plane, the intensity pattern and helical phase wavefronts of the $l = 1$ mode OAM beams for the ground plane case are obtained similarly. In Figure 5, more than one ring-shaped distribution is observed both in the intensity pattern (Figure 5(a)) and in the phase wavefront (Figure 5(b)), with the observation plane with a width of 1 km in the x-y direction formed by the sample window at $z = 1$ km.

Since the h height value is a variable of the multipath factor ($2cos(k_0hcos\theta)$ for the vertical polarization, $2jsin(k_0hcos\theta)$ for the horizontal polarization), it is clear that if the UCA has various heights, it will have different positions and a number of OAM pattern slices. Figure 6(a) shows the 3-D OAM beam pattern of the UCA located parallel to the $h = 3\lambda$ height from the infinitely sized superconducting ground plane. As seen in the Figure 6(a), 6 ($\frac{2(3\lambda))}{\lambda} = 6$) slices of OAM pattern are formed in the $\theta \in [0, \frac{\pi}{2}]$ range of the UCA located at a $h = 3\lambda$ height. The intensity pattern of the UCA, which is $h = 3\lambda$ above the ground plane in Figure 6(b), and the phase wavefront of the UCA, which is $h = 3\lambda$ above the ground plane in Figure 6(c) are observed with the observation window with a width of 1 km in the x-y direction formed by the sample window at $z = 1$ km. The phase wavefront and the intensity pattern with the "donut" shaped distribution of the OAM wave formed by the UCA at the $h = 3\lambda$ height over the ground are divided into two slices. The number of the OAM main pattern slices consists of 3 slices for $h = 5\lambda$ in the previous example, depending on the h height.

Similarly, the 3-D OAM beam pattern of the parallel-positioned UCA (at a height of $h = 7\lambda$) with respect to the infinitely sized superconducting ground plane is shown in Figure 7(a). It is clearly seen from Figure 7(a) that 14 OAM radiation beam slices are formed in the $\theta \in [0, \frac{\pi}{2}]$ interval for the situation where the UCA is located at a $h = 7\lambda$ height from the ground position. It is seen that the "ring" shaped distribution intensity pattern and phase wavefront of the main OAM wave generated by the UCA at a $h = 7\lambda$ height over the ground plane is divided into four slices. It can also be seen from the various examples above that the number of main OAM radiation beam slices varies in relation to the h height.

On the other hand, let's examine the multipath propagation effects of the OAM wave by considering the same circular array upright to the ground plane (Figure 2) and at the height of $h = 5\lambda$ over the infinitely sized superconducting ground plane. First, where the ground plane is not considered, the center of the UCA located upright to the x-y plane is located at a $h = 5\lambda$ height from the origin. The three-dimensional snapshot graph of the OAM beam with mode-1 obtained for the case where the ground plane is not taken into account is examined in Figure 8. It can be seen from Figure 8 that the UCA located upright to the x-y plane generates the stable OAM beam with mod-1 in the y-direction. Figure 8(a) shows the half wave shape of the OAM beam, while Figure 8(b) shows the full OAM beam. As can be seen from both figures, a uniform OAM beam is obtained in the y-axis direction, which is the normal of the UCA, in an isolated environment where there is no ground plane.

The 3-D OAM beam of UCA, which is located upright to the $h = 5\lambda$ height from the ground plane, has reflections from the superconducting ground plane with infinite dimensions in addition to direct propagation. In the case of multipath propagation, where there is the most fundamental reflected radiation as well as direct radiation, the radiated OAM beam is affected by the multipath factor. Therefore, in the OAM radiation generated by the UCA located upright to the ground plane, similarly, nulls are formed in the elevation plane that

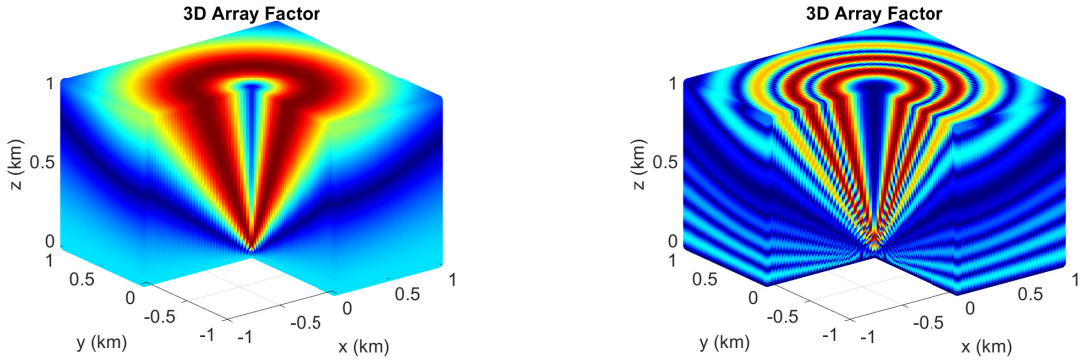

(a) (b)

Fig. 3. 3-D OAM beam pattern snapshot graph of UCA with mod-1, relative to the interval r at constant angle $\theta = 0$ and $\phi = 0$ (a) in the case where there is no ground plane, (b) in the case of the ground plane.

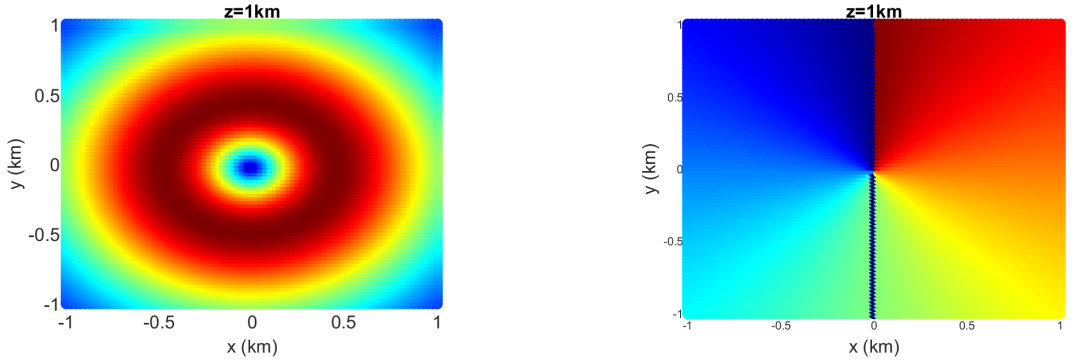

(a) (b)

Fig. 4. (a) intensity pattern and (b) helical phase wavefront at $z = 1$km of OAM beams produced by UCA with radius $a = 0.7\lambda$ located at the height of $h = 5\lambda$ from the origin for an isolated medium without a ground plane.

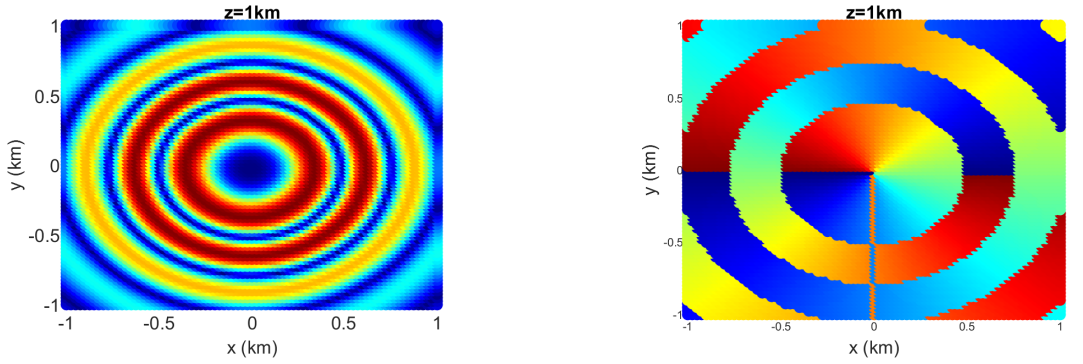

(a) (b)

Fig. 5. (a) intensity pattern and (b) helical phase wavefront at $z = 1$km of OAM beams produced by the parallel-positioned UCA (radius $a = 0.7\lambda$ and at a height of $h = 5\lambda$) with respect to the infinitely sized superconducting ground plane in the x-y plane.

divides the OAM beam into slices. Figure 9(a) and Figure 9(b) show the half and full OAM beams of the sliced OAM wave as a result of nulls resulting from the multipath effect, respectively. In both Figures, it can be seen that the UCA located uprightly at a height of $h = 5\lambda$ for the horizontal polarization case has $\frac{2(5\lambda))}{\lambda} = 10$ OAM radiation beam separate into segments in the $\theta \in [0, \frac{\pi}{2}]$ range.

Positioned both parallelly and uprightly to a superconducting ground plane with infinite dimensions, the OAM radiation beam of the UCA is segmented in the elevation plane depending on the height from the ground position. The number and position of nulls that separate into segments of the OAM radiation beam vary depending on the multipath factor.

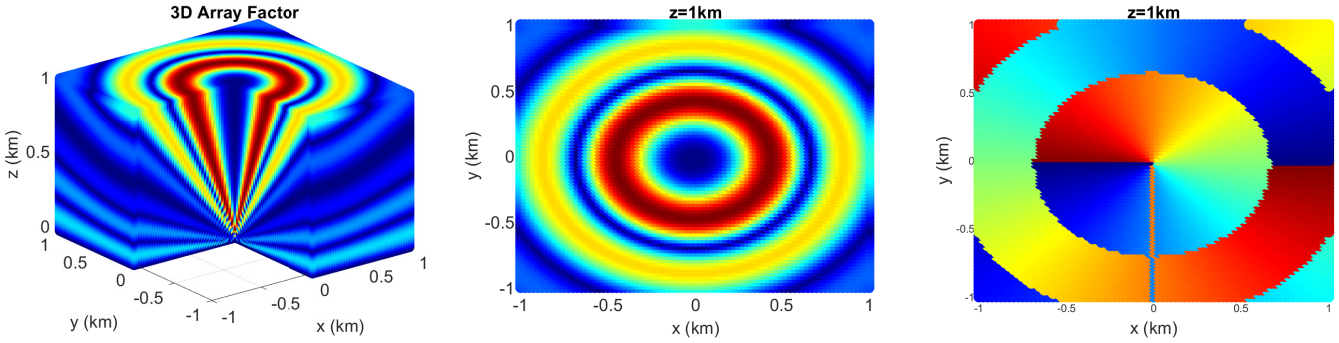

(a) (b) (c)

Fig. 6. (a) 3-D OAM beam pattern snapshot graph of the UCA with radius $a = 0.7\lambda$ located parallel to the $h = 3\lambda$ height from the infinitely sized superconducting ground plane in the x-y plane. (b) intensity pattern and (c) helical phase wavefront at $z = 1$km of OAM beams produced by UCA located parallel to the $h = 3\lambda$ height from the x-y plane.

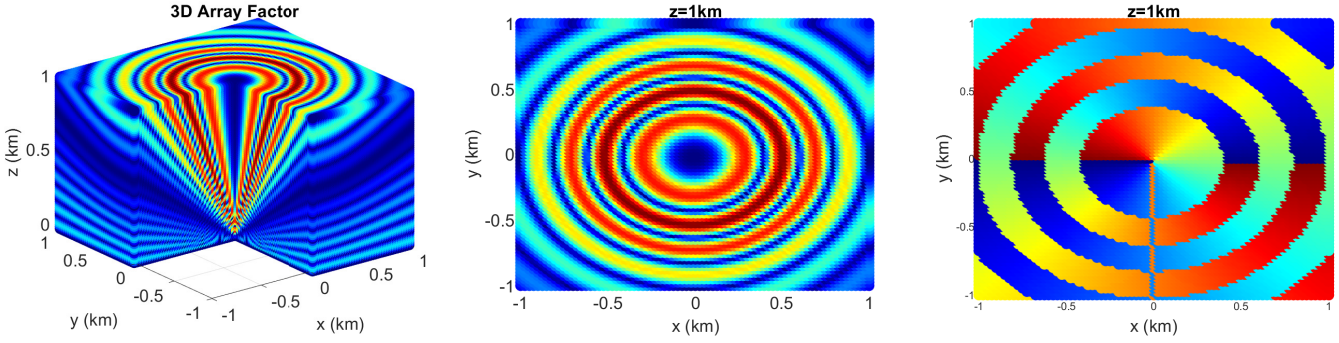

(a) (b) (c)

Fig. 7. (a) 3-D OAM beam pattern snapshot graph of the UCA with radius $a = 0.7\lambda$ located parallel to the $h = 7\lambda$ height from the infinitely sized superconducting ground plane in the x-y plane. (b) intensity pattern and (c) helical phase wavefront at $z = 1$km of OAM beams produced by UCA located parallel to the $h = 7\lambda$ height from the x-y plane.

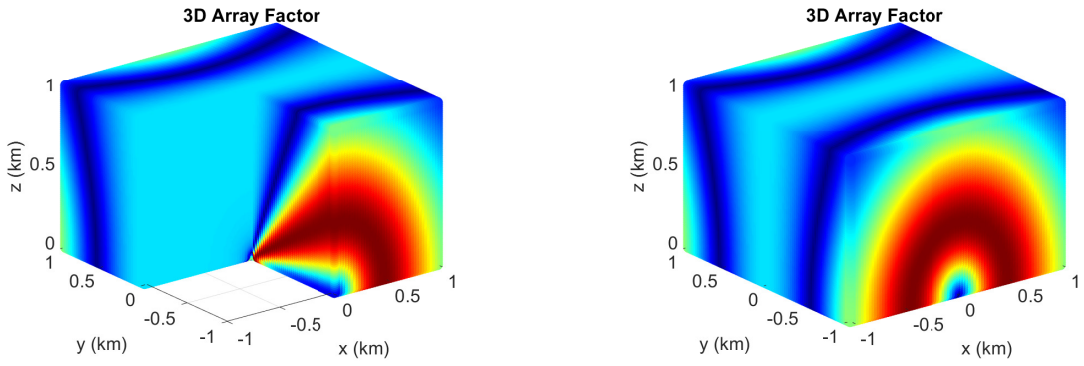

(a) (b)

Fig. 8. (a) Half and (b) a full 3-D snapshot graph of the OAM wave formed along the y-axis of the UCA located uprightly and at a $h = 5\lambda$ height from the x-y plane in the absence of the ground plane

IV. Conclusion

The multipath characteristic for an OAM beam containing one direct and one reflection path, with a more realistic approach compared to the isolated medium, is investigated in this study. In this sense, the total electric field at the observation point, which includes the direct and most fundamental reflected radiation, is derived from the parallel and upright-positioned UCA with respect to the infinitely sized superconducting ground plane. Unlike the electric field expression obtained in an isolated environment, the antenna element's field and the UCA array factor as well as the multipath factor are included. The OAM radiation model is segmented in the elevation plane due to the nulls generated by the multipath factor based on the height between the array and the ground position. As a result, the OAM radiation properties of UCA in an isolated environment and at a given height above the

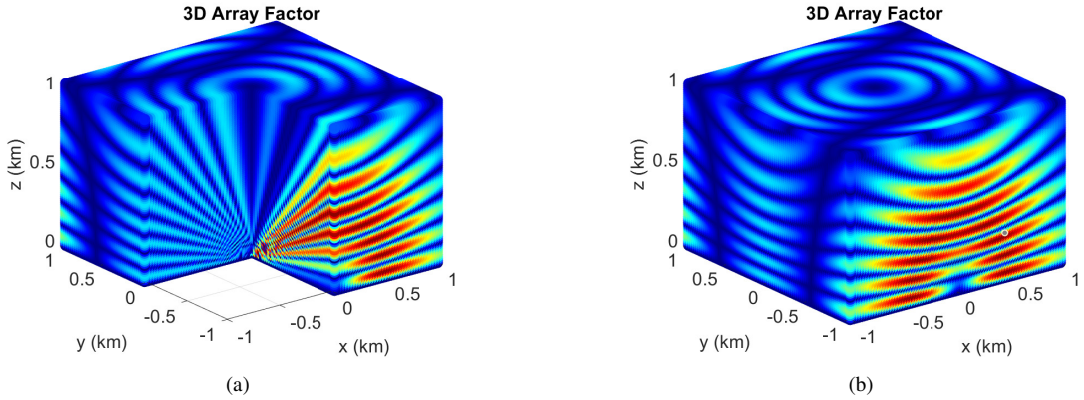

(a) (b)

Fig. 9. (a) Half and (b) a full 3-D snapshot graph of the OAM wave formed along the y-axis of the upright-positioned UCA (at a height of $h = 5\lambda$) with respect to the infinitely sized superconducting ground plane in the x-y plane

ground are analytically demonstrated by deriving theoretical expressions and comparative simulation results.

REFERENCES

[1] F. Tamburini, E. Mari, A. Sponselli, B. Thidé, A. Bianchini, and F. Romanato, "Encoding many channels on the same frequency through radio vorticity: first experimental test," *New Journal of Physics*, vol. 14, no. 3, p. 033001, Mar. 2012.

[2] F. E. Mahmouli and S. D. Walker, "4-gbps uncompressed video transmission over a 60-ghz orbital angular momentum wireless channel," *IEEE Wireless Communications Letters*, vol. 2, no. 2, pp. 223–226, 2013.

[3] A. E. Willner, "Communication with a twist," *IEEE Spectrum*, vol. 53, no. 8, pp. 34–39, 2016.

[4] R. Gaffoglio, A. Cagliero, G. Vecchi, and F. P. Andriulli, "Vortex waves and channel capacity: Hopes and reality," *IEEE Access*, vol. 6, pp. 19 814–19 822, 2018.

[5] S. Yu, N. Kou, J. Jiang, Z. Ding, and Z. Zhang, "Beam steering of orbital angular momentum vortex waves with spherical conformal array," *IEEE Antennas and Wireless Propagation Letters*, vol. 20, no. 7, pp. 1244–1248, 2021.

[6] Z. Yu, C. Han, Y. Zou, and X. Lu, "Location and angular velocity detection using a circular frequency diverse array radar," in *2021 IEEE Asia-Pacific Microwave Conference (APMC)*, 2021, pp. 58–60.

[7] J. Luo, S. Wang, and F. Wang, "Secure range-dependent transmission with orbital angular momentum," *IEEE Communications Letters*, vol. 23, no. 7, pp. 1178–1181, 2019.

[8] J. Ma, X. Song, Y. Yao, Z. Zheng, X. Gao, and S. Huang, "Secure transmission of radio orbital angular momentum beams based on the frequency diverse array," *IEEE Access*, vol. 9, pp. 108 924–108 931, 2021.

[9] G. X. e. a. Yan Yan, Long Li, "Multipath effects in millimetre-wave wireless communication using orbital angular momentum multiplexing," *Scientific Reports*, vol. 6, no. 3348, 2016.

[10] S. K. N. et al., "A review of orbital angular momentum vortex waves for the next generation wireless communications," *in IEEE Access*, vol. 10, pp. 89 465–89 484, 2022.

[11] C. F. J. Li, X. Pang, "Electromagnetic wave with oam and its potential applications in iot," in *Lecture Notes of the Institute for Computer Sciences, Social Informatics and Telecommunications Engineering*, vol. 316, 2020.

[12] L. Allen, M. W. Beijersbergen, R. J. C. Spreeuw, and J. P. Woerdman, "Orbital angular momentum of light and the transformation of laguerre-gaussian laser modes," *Phys. Rev. A*, vol. 45, pp. 8185–8189, Jun 1992. [Online]. Available: https://link.aps.org/doi/10.1103/PhysRevA.45.8185

[13] K. Liu, Y. Cheng, X. Li, Y. Qin, H. Wang, and Y. Jiang, "Generation of orbital angular momentum beams for electromagnetic vortex imaging," *IEEE Antennas and Wireless Propagation Letters*, vol. 15, pp. 1873–1876, 2016.

[14] R. Chen, H. Zhou, M. Moretti, X. Wang, and J. Li, "Orbital angular momentum waves: Generation, detection, and emerging applications," *IEEE Communications Surveys & Tutorials*, vol. 22, no. 2, pp. 840–868, 2020.

[15] Y. Wang, X. Sun, and L. Liu, "A concentric array for generating multimode oam waves," *Journal of Communications and Information Networks*, vol. 7, no. 3, pp. 324–332, 2022.

[16] M. Wulff, T. Zhang, L. Wang, H.-D. Brüns, and C. Schuster, "Simulating aperture coupling of oam waves through an infinite pec plane using efie-mom—part i: Validation and numerical accuracy," *IEEE Transactions on Electromagnetic Compatibility*, vol. 65, no. 5, pp. 1389–1399, 2023.

[17] B. Thidé, H. Then, J. Sjöholm, K. Palmer, J. Bergman, T. D. Carozzi, Y. N. Istomin, N. H. Ibragimov, and R. Khamitova, "Utilization of photon orbital angular momentum in the low-frequency radio domain," *Phys. Rev. Lett.*, vol. 99, p. 087701, Aug 2007. [Online]. Available: https://link.aps.org/doi/10.1103/PhysRevLett.99.087701

[18] U. M and T. A., "Generation of electron beams carrying orbital angular momentum," *Nature*, vol. 464, no. 7289, pp. 737–739, 2010.

[19] R. Niemiec, C. Brousseau, K. Mahdjoubi, O. Emile, and A. Ménard, "Characterization of an oam flat-plate antenna in the millimeter frequency band," *IEEE Antennas and Wireless Propagation Letters*, vol. 13, pp. 1011–1014, 2014.

[20] H.-H. Lv, Q.-L. Huang, X.-J. Yi, J.-Q. Hou, and X.-W. Shi, "Low-profile transmitting metasurface using single dielectric substrate for oam generation," *IEEE Antennas and Wireless Propagation Letters*, vol. 19, no. 5, pp. 881–885, 2020.

[21] M. Alibakhshi-Kenari, M. Naser-Moghadasi, R. Sadeghzadeh, B. S. Virdee, and E. Limiti, "Traveling-wave antenna based on metamaterial transmission line structure for use in multiple wireless communication applications," *AEU - International Journal of Electronics and Communications*, vol. 70, no. 12, pp. 1645–1650, 2016. [Online]. Available: https://www.sciencedirect.com/science/article/pii/S1434841116309086

[22] M. Wulff, L. Wang, H.-D. Brüns, and C. Schuster, "Simulating aperture coupling of oam waves through an infinite pec plane using efie-mom—part ii: Application and interpretation," *IEEE Transactions on Electromagnetic Compatibility*, vol. 65, no. 5, pp. 1400–1409, 2023.

[23] T. Yuan, Y. Cheng, H. Wang, and Y. Qin, "Beam steering for electromagnetic vortex imaging using uniform circular arrays," *IEEE Antennas and Wireless Propagation Letters*, vol. 16, pp. 704–707, 2017.

[24] M. Lin, Y. Gao, P. Liu, and J. Liu, "Theoretical analyses and design of circular array to generate orbital angular momentum," *IEEE Transactions on Antennas and Propagation*, vol. 65, no. 7, pp. 3510–3519, 2017.

[25] K. Liu, Y. Cheng, X. Li, Y. Qin, H. Wang, and Y. Jiang, "Generation of orbital angular momentum beams for electromagnetic vortex imaging," *IEEE Antennas and Wireless Propagation Letters*, vol. 15, pp. 1873–1876, 2016.

[26] L. Fang and R. M. Henderson, "Orbital angular momentum uniform circular antenna array design and optimization-based array factor," in *2019 IEEE Texas Symposium on Wireless and Microwave Circuits and Systems (WMCS)*, 2019, pp. 1–4.

[27] T. Yuan, H. Wang, Y. Qin, and Y. Cheng, "Electromagnetic vortex imaging using uniform concentric circular arrays," *IEEE Antennas and Wireless Propagation Letters*, vol. 15, pp. 1024–1027, 2016.

[28] Y. Qin, K. Liu, Y. Cheng, X. Li, H. Wang, and Y. Gao, "Sidelobe suppression and beam collimation in the generation of vortex electromagnetic waves for radar imaging," *IEEE Antennas and Wireless Propagation Letters*, vol. 16, pp. 1289–1292, 2017.

[29] U. Yesilyurt and H. K. Polat, "Helical circular array configurations for generation of orbital angular momentum beams," *IEEE Antennas and Wireless Propagation Letters*, vol. 22, no. 5, pp. 1139–1143, 2023.
[30] L. Wang, W. Park, C. Yang, H.-D. Brüns, D. G. Kam, and C. Schuster, "Wireless communication of radio waves carrying orbital angular momentum (oam) above an infinite ground plane," *IEEE Transactions on Electromagnetic Compatibility*, vol. 62, no. 5, pp. 2257–2264, 2020.
[31] U. Yesilyurt, I. Kanbaz, and E. Aksoy, "Effect of ground plane on power losses and efficiency for uniform period time modulated arrays," *IEEE Sensors Journal*, vol. 22, no. 4, pp. 3637–3647, 2022.
[32] ——, "Power losses and efficiency analysis of non-uniform time modulated arrays over a ground plane," *AEU - International Journal of Electronics and Communications*, vol. 146, p. 154106, 2022. [Online]. Available: https://www.sciencedirect.com/science/article/pii/S1434841122000036

Ugur Yesilyurt was born in Erzurum, Turkey, in 1990. He received a bachelor's degree from the Department of Electrical and Electronics Engineering, Atatürk University, Erzurum, in 2013, and the M.Sc. and Ph.D. degrees in electrical and electronics engineering from Gazi University, Ankara, Turkey, in 2018 and 2023, respectively. He is currently an Assistant Professor at Erzurum Technical University. His research interests include antenna radiation patterns, time-modulated antenna arrays, frequency-diverse arrays, orbital angular momentum, and antenna design.